NONLINEAR OPTICAL CHARACTERISTICS OF N,N'-BIS(SALICYLIDENE)-*p*-PHENYLENEDIAMINE: Z-SCAN TECHNIQUE AND QUANTUM MECHANICAL CALCULATIONS

Abdolrasoul Gharaati[1], Yasaman Abed[2*] and Fatemeh Mostaghni[3]

[1,2]Physics Department, Payame Noor University, Iran
[3]Chemistry Department, Payame Noor University, Iran

ABSTRACT. In this work, we have characterized the linear and nonlinear optical properties of N,N′-bis(salicylidene)-*p*-phenylenediamine (BSP) in both macroscopic and microscopic modes by using Z-scan technique and quantum chemical calculations. The microscopic nonlinear optical properties of BSP were investigated by density functional theory with the basis set of 6-311G++dp. Electronic properties such as frontier molecular energies, band-gap energy, electron affinity, hardness, softness, and ionization potential were evaluated. The calculation of microscopic quantities included first-order hyperpolarizability and natural bond orbitals showed the electron delocalization, which confirmed the nonlinear optical properties in this compound. The results of the absorption spectrum of BSP in DMSO, DMF, CH$_3$Cl solvents were shown that the dissolved sample in DMSO had better nonlinear properties than others. Then the macroscopic nonlinear properties of the sample were determined by the Z-scan technique. The values of the nonlinear refractive index (n$_2$), nonlinear absorption coefficient (β), and third-order nonsusceptibility of the sample in DMSO were, 0.09250×10^{-10} cm^2/W, -0.174×10^{-6} cm/W and 4.101× 10^{-5} esu, respectively. The two-photon absorption in this molecule has been enhanced by the donor–bridge–donor (D–π–D) architecture. The theoretical and experimental results concluded that BSP seems to be promising candidates for future photonic and optoelectronic devices.

KEY WORDS: Azo dye, Nonlinear optic, Hyperpolarizability, One photon absorption, Two photon absorption, Schiff bases

INTRODUCTION

The phenomenon that occurs as a result of modifying of the optical properties of a material system due to interaction with high-energy light is called nonlinear optics [1]. The first observation in the field of nonlinear optics whose discovery relied on the invention of the laser was second-harmonic generation (SHG) [2, 3].

In recent years, improvement of nonlinear optical (NLO) materials has been a growing interest due to their widespread usage in optical devices such as optical storage, optical-limiting optical switching, and information technology [4-10]. It has been observed that organic materials consist of delocalized conjugated π- electrons and a significant dipole moment have attracted tremendous attention motivated by their high absorption ability and applications in electronic, linear and nonlinear optics, sensors and biomedicine[11]. In conjugated organic materials, electrons in π bond are delocalized and have more motions rather than other electrons. In this case the π-bond electrons can easily move in the whole molecule space. The molecular structure of materials plays a significant role in the type of nonlinear optical behavior. Thus, further research has been carried for cheaper and more efficient materials [12]. Among organic compounds, Schiff bases have been noted for their electronic properties and good solubility in common solvents, as well as easy preparation methods and wide structural diversity [13-18].

Aromatic Schiff bases have also exhibited a broad range of NLO activities [19-24]. Aromatic Schiff bases are prepared from the condensation of aromatic amines and aromatic aldehydes. The

_____

*Corresponding author. E-mail: yasamanabed@gmail.com ; physics1396@gmail.com

characteristic functional group of the Schiff bases is called azo-methine or imine, which has a carbon- nitrogen double bond.

In this study, N,N′-bis(salicylidene)-*p*-phenylenediamine (BSP) as a symmetric aromatic Schiff base was synthesized, and its optical properties were investigated by z-scan technique and quantum chemical calculation. According to our knowledge, there are only a few reports on the nonlinear optical properties of BSP.

Quantum chemical calculation applied in the calculation of the structures and physicochemical properties of molecules. In the first step, we used TD-DFT quantum chemical calculations for determination of molecular hyperpolarizabilities of BSP that accelerate subsequent experimental studies. Then, the band-gap energy of the sample was calculated using the UV–Vis spectra, and the absorption coefficient and nonlinear refractive index were determined using the Z-scan technique.

EXPERIMENTAL

Synthesis of N,N'-bis(salicylidene)-p-phenylenediamine (BSP)

BSP was synthesized by the conventional condensation of 2-hydroxy benzaldehyde and 1,4-phenylene diamine. A methanolic solution (30 mL) of 2-hydroxy benzaldehyde (4.88 g, 40 mmol) was added to the 30 mL ethanolic solution of 1,4-phenylene diamine (2.16 g, 20 mmol). The mixture was refluxed for 5 hours. The orange precipitate was formed upon cooling. Then the precipitate was filtered, and washed with water. BSP crystals were obtained by recrystallization of the crude product from CH_2Cl_2. Yellow solid, yield 99%. ^{1}H NMR (400 MHz, DMSO-d6, ppm, 298 K): 13.07 (s, 2H), 9.03 (s, 2H), 7.57 (m, 8H), 6.99 (t, 4H). ^{13}C NMR (100 MHz, DMSO-d6, ppm, 298 K): 163.85, 160.98, 147.33, 134.05, 133.25, 123.24, 120.06, 119.89, 117.31. IR (KBr): 3438, 1612, 1571, 1508, 1495, 1457, 1430, 1407, 1372, 1324, 1286, 1213, 1191, 1163, 1149, 1131, 1037, 966, 903, 862, 828, 778, 764, 753, 735, 619, 562, 525, 487 cm^{-1}.

UV–Vis absorption and fluorescence spectroscopy

The absorption and emission spectra of the sample have been recorded on UV–Vis spectrophotometer (Perkin Elmer, Lama 35) and Perkin Elmer LS55 fluorescence spectrometer, respectively. Spectra were measured in dimethylsulfoxide (DMSO), dimethylformamide (DMF), and chloroform (CH$_3$Cl) solutions (1×10^{-4} M) in the range of 200-800 nm and corrected for background due to solvent absorption

Z-Scan measurement

Z-Scan technique, which is classified as self-focal process measurement methods was used measuring nonlinear refractive index of materials. In this method, a single laser beam is tightly focused onto a nonlinear sample medium. The sample moves along the focal point of the beam. This displacement in the Z-direction changes the transmittance of a nonlinear medium as a function of the sample position. The transmitted signal goes either directly or through an aperture to a detector. The transmissions with and without the aperture are plotted as a function of the sample position, these positions are called z-displacements. The Z-scan method consists of two open and closed aperture configurations that determine the nonlinear absorption coefficient β and the nonlinear refractive index n$_2$. The Z-scan experiments were performed using a Nd:YAG laser system as the excitation source emitting 5 ns 532 nm laser with a repetition rate of 10 Hz.

RESULTS AND DISCUSSION

Computational method

All quantum chemical calculations were carried out using the Gaussian 09 program [25]. TD-DFT calculations were performed by using the B3LYP functional and the usual 6-311++G (d,p) basis set.

Frontier molecular orbital analysis

The energy of HOMO indicates the electron-donating ability of a molecule, which is directly relate to the ionization potential. Whereas the energy of LUMO is the ability to accept electrons, relate to the electron affinity (A). Global hardness and softness are the most important properties for determination of the molecular stability and reactivity.

Electronic properties such as HOMO and LUMO energies, band gap energy, ionization potential (IP), electron affinity (EA), hardness (η), and softness (S), are summarized in Table 1. The small band gap energy indicated the BSP molecule is a semiconductor, and has a high polarizability.

Table 1. Theoretically computed HOMO and LUMO energies, bandgap energy (E_{gap}), hardness (η), softness (S), ionization potential (IP), and electron affinity (EA).

E_{HOMO} (eV)	E_{LUMO} (eV)	η (eV)	S (eV)	IP (kJ/mol)	EA (kJ/mol)	E_{gap} (eV)
-5.910	-2.367	3.543	0.282	570.215	228.391	3.542
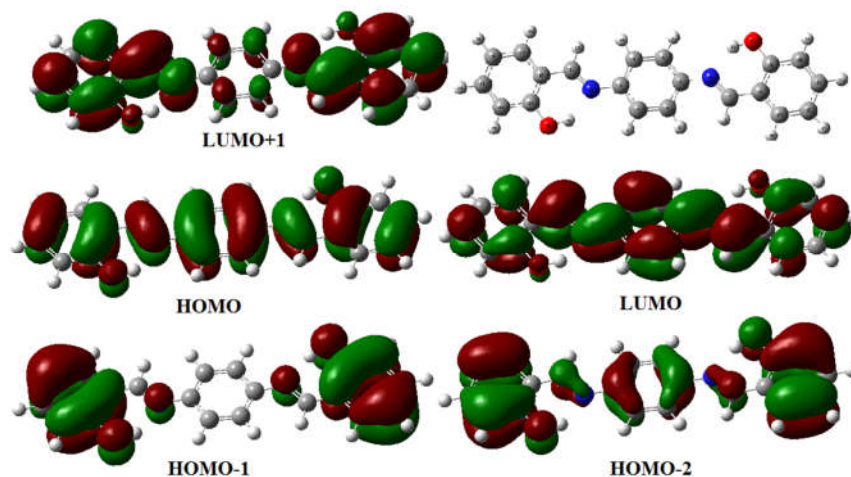
Figure 1. Molecular structure and Frontire orbitals of N,N'-bis(salicylidene)-*p*-phenylenediamine (BSP).

The orbitals involved in the main transitions are shown in Figure 1. The positive and negative phases are shown in red and green, respectively. As can be seen, in HOMO, the nonzero spin density occurs on the whole molecule. While, HOMO-1 is only delocalized on the two phenolic rings and HOMO-2 is mostly delocalized on C=N and two phenolic rings. By contrast, the majority of the electron cloud distribution of LUMO was most located on the central phenyl ring.

While, the electron cloud, of LUMO+1 was located on C=N and the two phenol rings. Consequently, electron transition from ground to excited states facilitates an electron density transfer and consequently, a change in the magnetic moment.

The light-harvesting efficiency (LHE) was approximately calculated from oscillator strength (f) using the following equation [26]:

$$LHE = 1 - 10^{-f} \tag{1}$$

Table 2. Excitation energies (E_{ex}), oscillator strengths (f), light harvesting efficiencies (LHE), and electronic transitions configurations of the title compound at TD-B3LYP/6-31G++(d,p) level in DMSO.

Excited State	E_{ex}	f	LHE	Transition assignment
83 -> 84 (S)	3.0473 eV 406.86 nm	1.2217	0.94	H→L (97.13%)
83 -> 85 (S)	3.5979 eV 344.60 nm	0.0062	0.014	H→L+1 (89.45%)
82 -> 84 (S)	3.8377 eV 323.07 nm	0.0251	0.056	H-1→L (89.63%)
81 -> 85 (S)	3.8377 eV 323.07 nm	0.0251	0.056	H-2→L+1 (5.22%)

As can be seen from Table 2, BSP showed the strongest absorptions at 406 nm (f = 1.2217), and 344 nm (f = 0.0062) and 323 nm (f = 0.0251). Two longer wavelength peaks be assigned to electron transition from HOMO to LUMO and LUMO+1, whereas the shorter wavelength is from HOMO-1 to LUMO. As expected, the low energy electronic excitation $\pi \rightarrow \pi^*$ be assigned with the 97.13% composition of the intense S_0–S_1 transition have strong ICT character. It was obvious that a dominant HOMO→LUMO transition caused the electron density increase on the N_{13} and N_{28} atoms, while that on the O_{35} and O_{37} atoms decreased.

One photon absorption

Asymmetry in the molecular charge distribution is represented by dipole moment. The direction of the dipole moment vector in the molecule depends on the centers of positive and negative charges.

As shown in Table 3, dipole moment is greater than zero, therefore the molecule is dipolar. When dipolar systems absorb photons with appropriate energy, transition of electrons occurs from the donor to the acceptor groups in the molecule; such a process is called intramolecular charge-transfer (ICT). However, the magnitude of the isotropic polarizability α and anisotropy of polarizability (Δα) are calculated using the polarization components [28] as follows:

$$\alpha_{ve} = \frac{1}{3}(\alpha_{xx} + \alpha_{yy} + \alpha\alpha_{zz}) \tag{2}$$

$$\Delta\alpha = \frac{1}{\sqrt{2}}\left[(\alpha_{xx} - \alpha_{yy})^2 + (\alpha_{xx} - \alpha_{zz})^2 + (\alpha_{yy} - \alpha_{zz})^2\right]^{1/2} \tag{3}$$

The isotropic polarizability (α), the anisotropy of the polarizability (Δα) of BSP are listed in Table 3.

Two photon absorption

The first hyperpolarizability (β), which is studied using second harmonic generation (SHG) is represented by two factors, namely β_{vec} and β_{tot}. β_{tot} refers to the total hyperpolarizability, defined as [28]:

$$\beta_{tot} = \left[\begin{matrix}(\beta_{xxx} + \beta_{xyy} + \beta_{xzz})^2 + (\beta_{yyy} + \beta_{yzz} + \beta_{yxx})^2 \\ + (\beta_{zzz} + \beta_{zxx} + \beta_{zyy})^2\end{matrix}\right]^{1/2} \tag{4}$$

and β_{vec} is the vector component of first hyperpolarizability reperesented by:

$$\beta_{vec} = \frac{(\beta_x\mu_x+\beta_y\mu_y+\beta_z\mu_z)}{\mu} \tag{5}$$

Also, the direction of charge transfer in the title compound was determined by the ratio of β_{vec} and β_{total} using the following equations [28]:

$$\cos\theta = \frac{\beta_{vec}}{\beta_{tot}} \tag{6}$$

The vector component of the polarizability, first hyperpolarizabilities and inplane non-linearity anisotropy (β) of BSP are listed in Table 3.

Table 3. The vector component of the polarizability, first hyperpolarizabilities and inplane non-linearity anisotropy (β) of BSP.

Parameters	a.u.	Parameters	a.u.
μ_x	0	β_{yxy}	0.000086
μ_y	0.00019	β_{yyy}	-0.02915
μ_z	1.41549	β_{xxz}	918.006
μ_{tot}	1.41549	β_{yxz}	51.4166
α_{xx}	768.650	β_{yyz}	-190.382
α_{yy}	325.995	β_{zxz}	-0.00838
α_{zz}	250.859	β_{zyz}	-0.00326
α_{yx}	5.08615	β_{zzz}	-423.773
α_{zx}	.003106	β_x	0.166244
α_{yz}	-0.00619	β_y	0.155766
α_{ave}	448.501	β_z	911.552
$\Delta\alpha$	484.691	β_{tot}	911.552
$\beta_\perp$	60.7701	β_{vec}	911.552
β_{xxx}	0.0637138	$\dfrac{\beta_{vec}}{\beta_{tot}}$	1
β_{xxy}	0.0843284		
$\langle\gamma\rangle$	-6152.15		

As can be seen in Table 3, BSP possesses an inplane non-linearity anisotropy that resulted of an appropriate ratio of off-diagonal β_{xyy} versus diagonal β_{xxx} tensorial component of β. Furthermore, the ratio of $\beta_{vec}/\beta_{total}$ in Table 3 is equal to 1, which indicated the unidirectional charge transfer in the title compound. Moreover, BSP can be used as potential NLO material since the significant value of $\mu\beta_0$.

Natural bonding orbital analysis

Natural bond orbital (NBO) analysis provides an efficient method for investigation of charge delocalizations within the molecule. NBO analysis has been performed on BSP in order to explain ICT in the molecule that associated with hyperpolarizabilities. NBO calculations were performed using NBO 3.1 program in the Gaussian 09 package by TD-DFT/B3LYP method.

The perturbation energies of donor-acceptor interactions are given in Table 4. The strong intramolecular hyperconjugate interaction is due to the interamolecular hydrogen bonds (LP $N_{13}\rightarrow\sigma^*$ H_{36}-O_{35}, LP $N_{25}\rightarrow\sigma^*$ H_{38}-O_{37}). Both nitrogens N_{13} and N_{25} work as donor via H_{36} and H_{38} to forming pseudo six-membered ring. In polar nonprotic solvents, double proton transfer in the complex of two BSP molecules takes place [29].

Another hyperconjugation interactions was duo to overlap between the π and π^* orbitals in aromatic rings, which has caused the stability of the molecule by intramolecular charge transfer. Furthermore, there was the electron donating from the lone pair of phenolic oxygens and C=N to the corresponding aromatic ring. Besides, some strong intermolecular interactions obtained with stable energy are listed in Table 5. The natural population analysis of the BSP showed the Lewis structure 97.164% and non-Lewis structure 2.625%.

Table 4. Second order perturbation theory analysis of the Fock matrix in NBO basis in BSP.

Donor NBO (i)	Acceptor NBO (j)	E(2)kcal/mol
LP N_{13}	σ^* H_{36}-O_{35}	45.65
LP N_{25}	σ^* H_{38}-O_{37}	45.64
LP O_{35}	π^* C_{16} - C_{18}	42.74
LP O_{37}	π^* C_{26} − C_{28}	42.74
π C_{20}-C_{21}	π^* C_{16} - C_{18}	22.9
π C_{30}-C_{31}	π^* C_{26} − C_{28}	22.9
π C_{16}-C_{18}	π^* C_{17} − C_{19}	21.94
π C_{17}-C_{19}	π^* C_{20} − C_{21}	21.94
π C_{26}-C_{28}	π^* C_{27} − C_{29}	21.94
π C_{27}-C_{29}	π^* C_{30} − C_{31}	21.94
π C_1-C_2	π^* C_3 − C_4	21.49
π C_3-C_4	π^* C_1 − C_2	21.15
π C_{16}-C_{18}	π^* N_{13} - C_{14}	21.13
π C_{26}-C_{28}	π^* C_7 - N_{25}	21.13
π C_3-C_4	π^* C_5 − C_6	19.9
π C_5-C_6	π^* C_3 − C_4	19.87
π C_1-C_2	π^* C_5 − C_6	19.72
π C_5-C_6	π^* C_1 − C_2	19.28
π C_{20}-C_{21}	π^* C_{17} − C_{19}	16.52
π C_{30}-C_{31}	π^* C_{27} − C_{29}	16.52
π C_{17}-C_{19}	π^* C_{16} − C_{18}	15.84
π C_{27}-C_{29}	π^* C_{26} − C_{28}	15.84
σ C_{18}-O_{35}	σ^* H_{36}-O_{35}	14.98
σ C_{28}-O_{37}	σ^* H_{38}-O_{37}	14.98
π C_{16}-C_{18}	π^* C_{20} − C_{21}	14.97
π C_{26}-C_{28}	π^* C_{30} − C_{31}	14.97
π C_3-C_4	π^* N_{13} - C_{14}	14.05
π N_{13}-C_{14}	π^* C_3 − C_4	13.39
π C_7-N_{25}	π^* C_1 − C_2	13.27
π C_1-C_2	π^* C_7 - N_{25}	10.16
LP N_{13}	π^* C_4 − C_5	7.59
LP N_{25}	σ^* C_1 - C_2	7.59
LP O_{35}	σ^* C_{16} − C_{18}	6.65
LP O_{37}	σ^* C_{26} - C_{28}	6.65
π C_7-N_{25}	π^* C_{26} − C_{28}	6.6

UV–Vis absorption and fluorescence spectroscopy

UV–Vis absorption and fluorescence spectra of BSP are shown in Figures 2 and 3. UV-Vis spectra showed absorption peaks at 327 nm, and 381 nm, which are attributed to $\pi \rightarrow \pi^*$ transition in enol and keto forms of BSP, respectively. The low-intensity n$\rightarrow \pi^*$ transition was completely overload by the intensive $\pi \rightarrow \pi^*$ transitions.
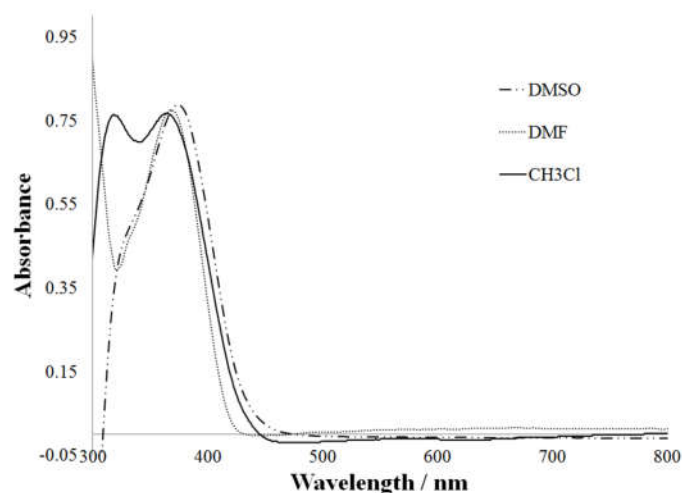
Figure 2. UV-Vis absorption spectra of BSP in in various solvents.
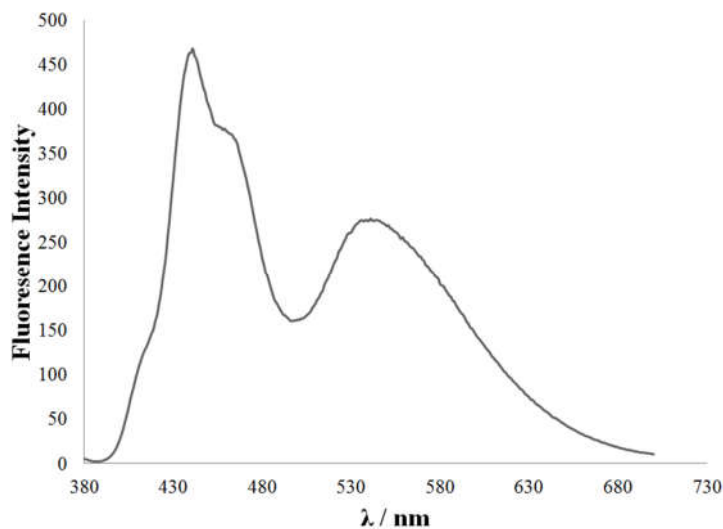
Figure 3. Fluorescence spectra of BSP in DMSO.

BSP is red-shifted with increasing solvent polarity. With increasing the polarity of solvent from CHCl$_3$ to DMSO, the tautomeric equilibrium enol-keto is shifted towards the keto form. As can be seen in Figure 2, peak intensity of keto form was greater than enol form. It is evident from the spectra that BSP showed the wide transparency in the visible region that enables it for the second harmonic generation required for all NLO material. The bandgap energy of BSP has been determined using the tauc relation [30] which is given by

$$(\alpha h\vartheta)^n = A(h\vartheta - E_g) \tag{7}$$

where α is absorption coefficient, hν is energy of photon, Eg is optical band gap, A is a transition probability constant, and n is a simple fraction which relates to the optical absorption process. For indirect allowed, direct allowed, indirect forbidden, and direct forbidden transitions, n is equal to 1/2, 2, 1/3, 2/3, respectively. The amount of energy gaps of BSP in DMSO, DMF and, CH_3Cl was calculated using the tauc equation. The amount of energy gaps of BSP in CH_3Cl, DMF and DMSO was E_g = 2.91, 2.79 and 2.49 eV, respectively. These results showed that the amount of energy gap has decreased with increasing solvent polarity. The reason for this decrease is that with increasing solvent polarity, the π orbital becomes more stable than the π* orbital.

Moreover, the maximum emission wavelengths of the sample occurred in the DMSO solvent at 438 and 451, and 528 nm as shown in Figure 3. The strong absorption at 528 nm is assigned to the keto form. The larger the wavelength of the emission than the maximum absorption wavelength is the result of re-combining part of the electron-hole in a non-radiant way through thermal radiation. Excited state intramolecular proton transfer (ESIPT) leads to a significant Stokes-shifted emission.

The difference between the maximum absorption wavelength and the maximum emission wavelength indicates the stokes shift [3] in the sample equal to 3419 cm^{-1}

$$\left(v_A - v_f\right) = \left(\frac{1}{\lambda_A} - \frac{1}{\lambda_F}\right) \times 10^7 \quad (cm^{-1}) \tag{8}$$

where v_A and v_f are absorption and emission wavenumber , λ_A and λ_f are the maximum absorption and emission wavelength.

Nonlinear refractive index

Figure 4 shows the observed transmittance versus sample position concerning to the focal point. As can be seen in Figure 4, we have a peak followed by a valley due to the beam irradiance was increased at the aperture. The nonlinear refractive index behavior of the sample is equivalent to the formation of an induced negative lens self-defocusing (negative).Therefore BSP had the negative nonlinearity and acted as a concave lens.
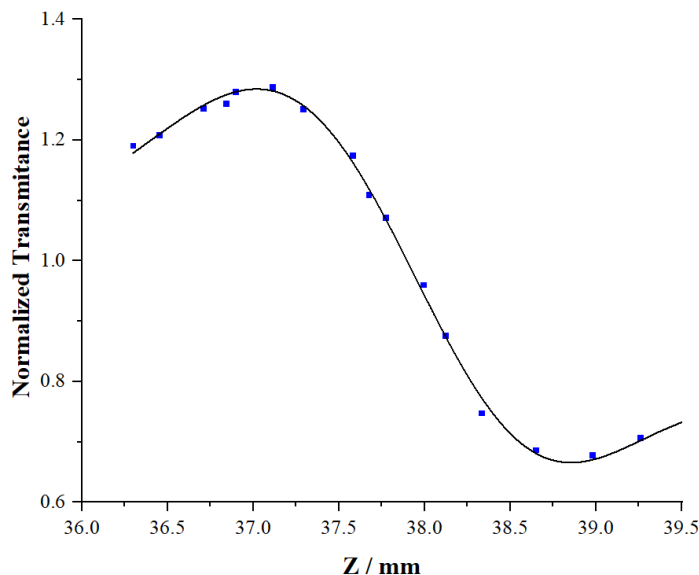
Figure 4. Closed aperture Z-Scan data for BSP solution.

Furthermore, the nonlinear refractive index (n_2) was be determined by the difference between the normalized peak and valley transmittance ΔT_{p-v} using the following equations [31]:

$$n_2 = \frac{\lambda(\Delta T_{p-v})}{0.406(1-S)^{0.25}(2\pi I_0)(\frac{[1-\exp(-\alpha L)]}{\alpha})} \tag{9}$$

where I_0 is the peak intensity at the focus as follows:

$$I_0 = \frac{2p}{\pi\omega^2} \tag{10}$$

and linear absorption

$$\alpha = -\frac{1}{L}\ln\left(\frac{P}{P_0}\right) \tag{11}$$

Linear transition S is then related to the radius of aperture (r_a) and the radius of the beam at the aperture (ω_a) by:

$$S = 1 - exp\left(\frac{-2r_a^2}{\omega_a^2}\right) \tag{12}$$

The nonlinear refractive index n_2 has been calculated from equations 8 to 11 and presented in Table 5.

Nonlinear absorption coefficient

In Figure 5 the normalized transmittance of open aperture Z-scan at wavelengths 532 nm was plotted as a function of sample position.
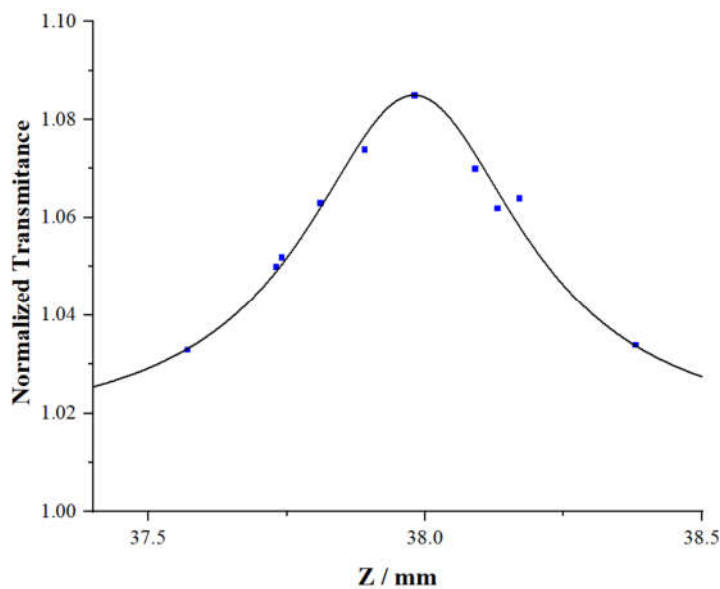
Figure 5. Open aperture Z-scan data for para red solution.

As shown in this figure, the open aperture curve indicates a peak shape which is a signature of a negative nonlinear absorption (NLA) coefficient.

The nonlinear absorption coefficient of the BSP can be easily calculated from this curve, using the following equations [28, 32].

$$(z, s = 1) = \sum_{m=0}^{\infty} \frac{\left[\frac{\beta I_0 L_{eff}}{1+\left(\frac{Z}{Z_0}\right)^2}\right]^m}{(m+1)^{\frac{3}{2}}} \tag{13}$$

where

$$Z_0 = \frac{K\omega_0^2}{2} \tag{14}$$

In the above equations, Z/Z_0 is the diffraction length of the Gaussian beam, I_0 is the peak intensity at the focus, T is the total transmittance, β is NLA coefficient, and L_{eff} is the effective thickness of the sample, it can be related related to α by equation 3.

$$L_{eff} = \frac{[1-\exp(-\alpha L)]}{\alpha} \tag{15}$$

where

$$\alpha = -\frac{1}{L}\ln\left(\frac{P}{P_0}\right) \tag{16}$$

The nonlinear absorption coefficient of BSP is tabulated in Table 5.

Third order susceptibility χ(3)

The real and imaginary parts of the third-order susceptibility $\chi^{(3)}$ are related to the value of nonlinear refractive index n_2 and nonlinear absorption coefficient β, respectively using the following equations [33]:

$$Re\chi^{(3)}(esu) = \left(\frac{10^{-4}\varepsilon_0 c^2 n_0^2}{\pi}\right)n_2, \ in \ \left(\frac{cm^2}{W}\right) \tag{17}$$

$$Im\chi^{(3)}(esu) = \left(\frac{10^{-2}\varepsilon_0 c^2 n_0^2 \lambda}{4\pi^2}\right)\beta, \ in \ \left(\frac{cm}{W}\right) \tag{18}$$

where n_0 is the linear refractive index, c is the speed of light in vacuum, and ε_0 is the vacuum permittivity.

The absolute value of the third-order nonlinear optical susceptibility can be obtained by:

$$\left|\chi^{(3)}\right| = \{[Re(\chi^{(3)})]^2 + [Im(\chi^{(3)})]^2\}^{1/2} \tag{19}$$

The values of the third-order nonlinear susceptibility, and other optical parameters obtained for BSP are listed in Table 5.

Table 5. Calculated third order nonlinear optical parameters of BSP.

$\chi^{(3)} \times 10^{-5}$ esu	Im $(\chi^{(3)}) \times 10^{-5}$ esu	Re $(\chi^{(3)}) \times 10^{-5}$ esu	$\beta \times 10^{-6}$ cm/W	$n_2 \times 10^{-10}$ cm^2/W
4.101	-4.07	0.511	-0.174	0.09295

As can be seen in Table 5, BSP exhibited large third-order susceptibilities with a magnitude of the order of 10^{-5} esu.

CONCLUSION

In this work, we reported the nonlinear optical properties analyses of BSP. Density functional theory (TD-DFT) has been employed to study the nonlinear optical properties of BSP, which was investigated with the basis set of 6-311G++dp.

The results of Frontier molecular orbital analysis showed the large ICT in BSP molecules. Besides, the dipole moment and total first static hyperpolarizability of the BSP molecule were found to be 1.41549 D and 911.552 a.u., respectively.

Also, hyper conjugative interactions and charge delocalization have been analyzed using natural bond orbital analysis. The strongest electron donation has occurred from a lone pair of nitrogen atoms to the anti-bonding acceptor (OH phenolic) orbitals.

Examination of the UV spectrum showed that increasing the solvent polarity makes the energy of the excited state π^* more stable than the π state in the $\pi \rightarrow \pi^*$ transition. Moreover, this stability shifts the peak of the absorption spectrum toward longer wavelengths, and reduces the energy bandgap of the sample dissolved in DMSO solvent compared to other samples. As a result, this solvent is a better candidate for the study of nonlinear properties. The experimental result of Z-scan also validates the NLO behavior of BSP. The nonlinear refractive index and nonlinear absorption coefficient have been measured for BSP in DMSO using the Z scan technique. The results showed that the nonlinear refractive index and nonlinear absorption of BSP could be explained by thermally induced refractive index change and reverse saturation effects respectively. The two-photon absorption in this molecule has been enhanced by the donor–bridge–donor (D–π–D) architecture. The theoretical and experimental results conclude that BSP seems to be promising candidates for future photonic and optoelectronic devices.

AKNOWLEDGMENTS

REFERENCES

1. Guo, Y.; Kao, C.K.; Lie, H.; Chiang, K.S. *Nonlinear Photonics*, Springer: Berlin; **2002**.
2. Nalwa, H.S. *Handbook of Advanced Electronic and Photonic Materials and Devices*, Academic Press: New York; **2001**.
3. Dmitriev, V.G.; Gurzadyan, G.G.; Nikogosyan, D.N. *Handbook of Nonlinear Optical Crystals*, Springer-Verlag: Berlin; **2013**.
4. Gandhimathi, R.; Dhanasekaran, R. Structural, thermal, mechanical and Z-scan studies on 4-nitrophenol single crystals. *Cryst. Res. Technol*. **2012**, 47, 385-390.
5. Zidan, M.D.; Allaf, A.W.; Allahham, A.; Al-Zier, A. Nonlinear optical investigation of molybdenum phenanthroline complex. *J. Optoelectron. Adv. Mater.* **2021**, 23, 285-292.
6. Ghanem, A.; Zidan, M.D.; EL-Daher, M.S. Investigation of the optical nonlinear properties of chlorophyll B using Z-scan, Iran. *J. Sci. Technol. Trans. A: Sci.* **2021**, 45, 761-765.
7. Wang, C.; Dong, H.; Hu, W.; Liu, Y.; Zhu, D. Semiconducting π-conjugated systems in field-effect transistors: a material odyssey of organic electronics. *Chem. Rev*. **2012**, 112, 2208-2267.
8. Zhang, F.; Wu, D.; Xu, Y.; Feng, X. Thiophene-based conjugated oligomers for organic solar cells. *J. Mater. Chem.* **2011**, 21, 17590-17600.
9. Barragan, E.; Poyil, A.N.; Yang, C.H.; Wang, H.; Bugarin, A. Metal-free cross-coupling of π-conjugated triazenes with unactivated arenes via photoactivation. *Org. Chem. Front*. **2019**, 6, 152-161.
10. Lu, J.; Pan, Q.; Zhu, S.; Liu, R.; Zhu, H.; Ligand-mediated photophysics adjustability in bis-tridentate Ir(III) complexes and their application in efficient optical limiting materials. *Inorg. Chem*. **2021**, 60, 12835-12846.

11. Dragonetti, C.; Colombo, A.; Fontani, M.; Marinotto, D.; Nisic, F.; Righetto, S.; Roberto, D.; Tintori, F.; Fantacci, S. Novel fullerene platinum alkynyl complexes with high second-order nonlinear optical properties as a springboard for NLO-active polymer films. *Organomet.* **2016**, 35, 1015-1021.

12. Paradopoulos, M.G.; Sadlej, A.J.; Leszynski, J. *Non-linear Optical Properties of Matter from Molecules to Condensed Phases*, Springer: Dordrecht, Netherlands; **2006**.

13. Wazzan, N.; Safi, Z. DFT calculations of the tautomerization and NLO properties of 5-amino-7-(pyrrolidin-1-yl)-2,4,4-trimethyl-1,4-dihydro-1,6-naphthyridine-8-carbonitrile (APNC). *J. Mol. Struct.* **2017**, 1143, 397-404.

14. Pron, A.; Gawrys, P.; Zagorska, M.; Djurado, D.; Demadrille, R. Electroactive materials for organic electronics: preparation strategies, structural aspects and characterization techniques. *Chem. Soc. Rev.* **2010**, 39, 2577-2632.

15. Wojciechowski, A.; Raposo, M.M.; Castro, M.C.; Kuznik, W.; Fuks-Janczarek, I.; Pokladko-Kowar, M.; Bureš, F. Nonlinear optoelectronic materials formed by push–pull (bi) thiophene derivatives functionalized with di (tri) cyanovinyl acceptor groups. *J. Mat. Sci: Mat. Elec.* **2014**, 25, 1745-1750.

16. Mishra, A.; Bäuerle, P. Small molecule organic semiconductors on the move: promises for future solar energy technology. *Angew. Chem. Int. Ed.* **2012**, 51, 2020-2067.

17. Zielinska, B.D.; Barwiolek, M.; Cassagne, C.; Boudebs, G. Nonlinear optical study of Schiff bases using Z-scan technique. *Opt. Laser Technol.* **2020**, 124, 105968.

18. Sathiyamoorthy, K.; Vijayan, C.; Kothiyal, MP. Low power optical limiting in ClAl-phthalocyanine due to self defocusing and self phase modulation effects. *Opt. Mater.* **2008**, 31, 79-86.

19. Sahraei, A.; Kargar, H.; Hakimi, M., Applications and attributes of nickel(II) Schiff base complexes derived of phenylenediamine. *Bulg. Chem. Commun.* **2016**, 48, 33-43.

20. Gomathi, V.; Selvameena, R. Synthesis, structural analysis and antimicrobial screening of Mn(II) complexes of Schiff bases. *J. Mex. Chem. Soc.* **2022**, 66, 70-78.

21. Safin, D.A.; Babashkina, M.G.; Garcia, Y. Crown ether-containing Schiff base as a highly efficient "turn-on" fluorescent sensor for determination and separation of Zn^{2+} in water. *Dalton Trans.* **2013**, 42, 1969-1972.

22. Mostaghni, F. 4-(4,5-Diphenyl-1H-imidazole-2-yl)phenol: Synthesis and estimation of nonlinear optical properties using Z-scan technique and quantum mechanical calculations, *Acta Chim. Slov.* **2021**, 68, 170-177.

23. Feng, Y.; Cheng, J.; Zhou, L.; Zhou, X.; Xiang, H. Ratiometric optical oxygen sensing: A review in respect of material design. *Analyst* **2012**, 137, 4885-4901.

24. Boudebs, G.; Besse, V.; Cassagne, C.; Leblond, H.; de Araújo, C.B. Nonlinear characterization of materials using the D4σ method inside a Z-scan 4f-system, *Optics Lett.* **2013**, 38, 2206-2208.

25. Frisch, M.J.; Trucks, G.W.; Schlegel, H.B.; Scuseria, G.E.; Robb, M.A.; Cheeseman, J.R.; Scalmani, G.; Barone, V.; Petersson, G.A.; Nakatsuji, H.; Li, X.; Caricato, M.; Marenich, A. V.; Bloino, J.; Janesko, B.G.; Gomperts, R.; Mennucci, B.; Hratchian, H.P.; Ortiz, J.V.; Izmaylov, A.F.; Sonnenberg, J.L.; Williams-Young, D.; Ding, F.; Lipparini, F.; Egidi, F.; Goings, J.; Peng, B.; Petrone, A.; Henderson, T.; Ranasinghe, D.; Zakrzewski, V.G.; Gao, J.; Rega, N.; Zheng, G.; Liang, W.; Hada, M.; Ehara, M.; Toyota, K.; Fukuda, R.; Hasegawa, J.; Ishida, M.; Nakajima, T.; Honda, Y.; Kitao, O.; Nakai, H.; Vreven, T.; Throssell, K.; Montgomery Jr. J.A.; Peralta, J.E.; Ogliaro, F.; Bearpark, M.J.; Heyd, J.J.; Brothers, E.N.; Kudin, K.N.; Staroverov, V.N.; Keith, T.A.; Kobayashi, R.; Normand, J.; Raghavachari, K.; Rendell, A.P.; Burant, J.C.; Iyengar, S.S.; Tomasi, J.; Cossi, M.; Millam, J.M.; Klene, M.; Adamo, C.; Cammi, R.; Ochterski, J.W.; Martin, R.L.; Morokuma, K.; Farkas, O.; Foresman, J.B.; Fox, D.J. Gaussian, Inc.: Wallingford, CT; **2016**.

26. Wang, H.; Liu, Q.; Liu, D.; Su, R.; Liu, J.; Li, Y. Computational prediction of electronic and photovoltaic properties of anthracene-based organic dyes for dye-sensitized solar cells. *Int. J. Photo.* **2018**, 4764830.
27. Machado, D.F.; Lopes, T.O.; Lima, I.T.; da Silva Filho D.A.; de Oliveira, H.C. Strong solvent effects on the nonlinear optical properties of Z and E isomers from azo-enaminone derivatives. *J. Phys. Chem. C* **2016** , 120, 17660-17669.
28. Jayabharathi, J.; Thanikachalam, V.; Devi, K.B.; Perumal, M.V. Optical properties of organic nonlinear optical crystal—A combined experimental and theoretical study. *Spectrochim. Acta, Part A.* **2012**, 86, 69-75.
29. Ziółek, M.; Burdzinski, G.; Karolczak, J. Influence of intermolecular hydrogen bonding on the photochromic cycle of the aromatic Schiff base N,N′-bis(salicylidene)-*p*-phenylenediamine in solution. *J. Phys. Chem. A* **2009** , 113, 2854-2864.
30. Van Stryland, E.W.; Sheik-Bahae, M. *Characterization Techniques and Tabulations for Organic Nonlinear Materials*, Marcel Dekker, Inc.: New York; **1998**; p 655.
31. Mostaghni, F.; Abed, Y. Synthesis and investigation of nonlinear optical properties of Para Red: Z-scan technique and quantum mechanical calculations. *Mater. Sci. Poland* **2018**, 36, 445-451.
32. Sutherland, R.L. *Handbook of Nonlinear Optics*, CRC Press: New York; **2003**.
33. Sheik-Bahae, M.; Said, A.A.; Wei, T.H.; Hagan, D.J. *IEEE J. Quan. Elec.* **1990**, 26, 760-769.